ACS APPLIED POLYMER MATERIALS

pubs.acs.org/acsapm Article

ABA Block Copolyester Thiol−Ene Resin From Triethylborane-Assisted Ring-Opening Copolymerization

Warrick Ma, Paula G. Miller, and Yadong Wang*

Cite This: https://doi.org/10.1021/acsapm.3c02745 Read Online

ACCESS | Metrics & More | Article Recommendations | Supporting Information

ABSTRACT: Leveraging metal-free ring-opening copolymerization catalyzed by a triethylborane and phosphazene base, we have developed a cytocompatible, thiol−ene-based block copolyester photoresin (BC1) with an ABA triblock architecture. A sebacate-derived polyester acting as the chain transfer agent improves the scalability of ring-opening copolymerization and enables the direct, facile synthesis of functional sebacate-derived polyesters by circumventing the conventional high-temperature polycondensation that will often destroy reactive functional groups. BC1's ABA block copolymer design enables tunable elasticity, and its surface property supports the proliferation of human umbilical vein endothelial cells better than polycaprolactone, a polyester with a well-established safety record. The polymerization approach presented in this work expands the potential of sebacate-derived materials and will inspire the development of more elastic photoresins that incorporate safe, renewable, and affordable feedstocks such as sebacic acid and other long-chain aliphatic carboxylic acids.

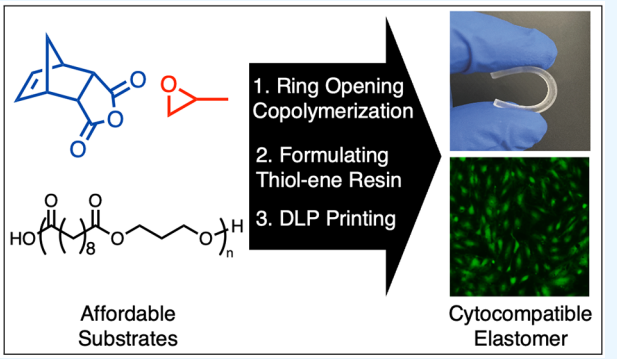

KEYWORDS: *DLP, 3D printing, ROCOP, click chemistry, polyester, thiol−ene, cytocompatible, elastomer*

INTRODUCTION

Digital light processing (DLP), a three-dimensional (3D) additive manufacturing technique, is low-cost, rapid, and high-resolution.[1−7] It enables the precise fabrication of customized devices and just-in-time prototypes. Available DLP resins, however, mostly comprise monomeric and/or oligomeric (meth)acrylates,[1] with their leachates, be that uncured monomers or additives, causing significant cell death *in vitro* and *in vivo*.[8−10] Even commercial resins certified as biocompatible leach toxic monomers and additives, such as surfactants and plasticizers, are used to make the cured resin more flexible.[8,9] Postprinting treatments such as extensive washing, UV postcuring, heat treatment, and coating with biocompatible materials ameliorate some of the toxicity concerns.[2,8,9] Furthermore, these treatments often significantly lengthen the fabrication process, contradicting the premise of rapid prototyping. As a result, despite additive manufacturing's many promises, the healthcare community has been slow to adapt.

In recent years, thiol−ene resins have been proposed to be a more biocompatible alternative. Particularly, thiol-norbornene click chemistry is biorthogonal, making possible a wide range of bioinks that incorporate living cells in the resin.[10,11] But their difficult synthesis and purification, and the resultant high cost, limit their potential for commercial success. 4Degra by 4D Biomaterials is the first commercialized thiol-norbornene resin.[4,12] It comprises polycarbonate with pendant allyl and norbornene groups, synthesized via base-catalyzed ring-opening polymerization of respective cyclic carbonate monomers. 4Degra, therefore, has properties that many acrylate-based materials lack: shape memory, biodegradability, and tunable elasticity. Polypropylene fumarate (PPF) is another notable example. Although PPF can engage in free radical cross-linking as (meth)acrylate does, thiol−ene cross-linking of PPF can yield soft materials with high elasticity, rather than the rigid materials generated by free radical cross-linking of fumarate.[13−16] Ring-opening copolymerization (ROCOP) of maleic anhydride and propylene epoxide (PO), with initiators such as propargyl alcohol and meso-erythritol, affords end-functionalized and star-shaped PPF, respectively.[14,17,18] The former conjugates with cell adhesive GRGDS peptides to improve its performance as a tissue engineering scaffold; the latter exhibits reduced viscosity compared to its linear counterpart, enabling 3D printing of PPF with a higher molecular weight.

These two examples demonstrate the utility of ring-opening polymerization in developing the next-generation photoresin.[5,19] It is milder and faster than step-growth poly-

Received: November 10, 2023
Revised: December 20, 2023
Accepted: December 21, 2023

Scheme 1. Workflow Illustrating the Synthesis of Poly(PO-*alt*-CPMA)-b-PPS-b-poly(CPMA-*alt*-PO) via ROCOP of CPMA and PO, the Formulation of BC1, and Its Resultant DLP 3D Printing (Scale Bar 1 cm)[a]

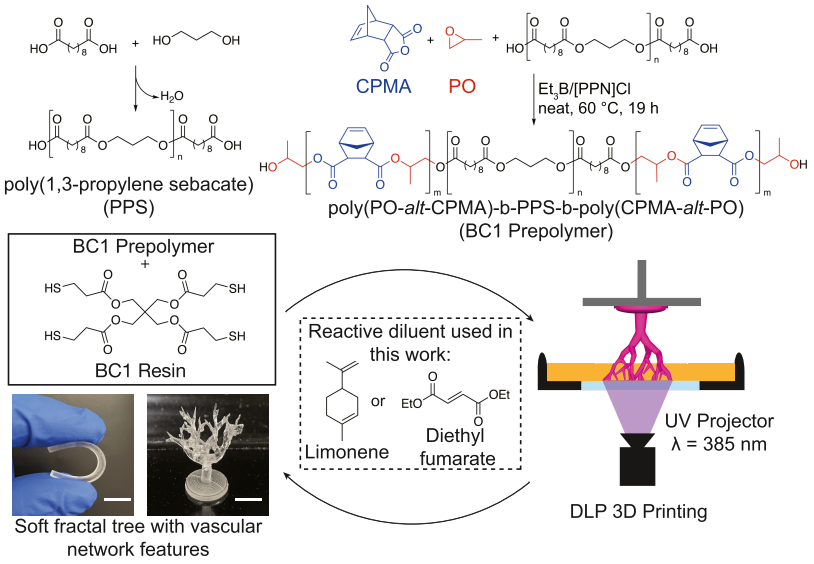

[a]PPS is synthesized by polycondensation of sebacic acid and 1,3-propanediol first under nitrogen gas for 3 h at 160 °C and then under vacuum for 2 h at 210 °C. To generate a photo-cross-linked network, pentaerythritol tetrakis(3-mercaptopropionate) (PETMP) was chosen as the thiol cross-linker and phenylbis(2,4,6-trimethylbenzoyl)phosphine oxide (TPO) as the photoinitiator. Ethyl acetate was used as the inert diluent for small-scale resin preparation to generate tensile testing specimens. Reactive diluents like limonene and diethyl fumarate were used to formulate resin for 3D printing.

condensation, the original method of synthesizing PPF.[13] Without it, precise control over polymer architecture, molecular weight, end-group functionality, and incorporation of heat-labile groups would be difficult. Many groups are devoted to developing new catalysts, especially for ROCOP of cyclic anhydride and epoxide.[20−24] Among the most active catalysts are metal-salen complexes and organoborons, yielding an alternating copolyester with molecular weight as high as 94.5 kDa.[20,22] They generally show high activity toward bicyclic and tricyclic carboxylic anhydride but lower activity toward many biologically relevant monomers such as succinic anhydride, glutaric anhydride, adipic anhydride, etc. due to their lower ring strain.[25,26] For other long-chain dicarboxylic acids such as sebacic acid and azelaic acid, both of which are FDA-approved and with extensive uses in synthesizing bioresorbable polyesters,[27,28] entropy simply does not favor the formation of cyclic, monomeric anhydride.[29] Synthesizing these polyesters, therefore, still requires high-temperature polycondensation. Although low-temperature variants exist—such as those catalyzed by Novozyme 435 (immobilized lipase from Candida Antarctica), which requires a temperature up to 80 °C,[30,31] or carbodiimides which can take place at room temperature,[32−34] —they can suffer from other drawbacks. Novozyme 435 is relatively expensive, among other issues that arise from the lipase immobilization process.[35] Carbodiimides-mediated polycondensation often needs reactants such as 4-dimethylaminopyridine and have poor atomic efficiency because these reagents need to be added in near stoichiometric amount and yield the corresponding urea side product.[32−34]

ROCOP can bridge this reactivity gap by transferring the reactivity to protic, polymeric initiators containing biologically relevant diacids.[36] Using the recent advent of metal-free, Lewis-pair-catalyzed ROCOP, we developed a tandem synthesis of the ABA triblock copolyester photoresin (BC1) strictly using widely commercially available monomers: sebacic acid, 1,3-propanediol, *cis*-5-norbornene-endo-2,3-dicarboxylic anhydride (CPMA), and propylene oxide. BC1 shows high fidelity on a desktop 3D printer, overcoming the suction cup effect and overcuring to produce challenging structures. The metal-free catalysis and efficient thiol−ene cross-linking not only minimize the amount of toxic leachates but render BC1's surface favorable to the proliferation of human umbilical vein endothelial cells (HUVECs), even more so than the FDA-approved polycaprolactone (PCL). To our knowledge, this is the first practical application of polyesters synthesized via ROCOP mediated by a triethylborane (Et_3B)-bis-(triphenylphosphine)iminium chloride ([PPN]Cl) catalyst pair. We believe that this strategy will expand the repertoire of biocompatible resins at scale and lead to functional materials with precisely controlled polymer architectures using biologically relevant diacid and diol monomers.

RESULTS AND DISCUSSION

PPS Synthesis and Characterization. According to our prior work on DLP 3D printing resins derived from acrylate-functionalized poly(glycerol sebacate),[37] sebacate-based polyesters' flexible octamethylene chains contribute to their elasticity. Despite these classes of materials' attractive elasticity and rapid photocuring, the high reaction temperature (120−220 °C) of melt condensation renders their direct synthesis impossible, as it often causes premature thermal cross-linking of the highly reactive acrylate.[38]

Chain extension of polyesters under mild conditions circumvents this limitation and enables direct functionalization of aliphatic polyesters by many reactive functional groups. Specifically, ROCOP of cyclic anhydrides and epoxides furnishing UV reactive functional groups, producing perfectly alternating block copolyesters with high molecular weights (M_n > 10 kDa) and low dispersity ($Đ$ < 1.3).[5,36] Lewis pair catalysts that are compatible with protic chain transfer agents (CTAs)

https://doi.org/10.1021/acsapm.3c02745
ACS Appl. Polym. Mater. XXXX, XXX, XXX−XXX

enable this by chain extension of CTAs and sequential addition approaches.[5] We synthesized PPS macroCTA by melt condensation of 1.05 equiv of sebacic acid and 1 equiv of 1,3-propanediol (Scheme 1). The 0.05 equiv excess is empirically chosen to compensate for the sublimation of sebacic acid. Gel permeation chromatography (GPC) calibrated with polystyrene standards revealed a series of low molecular weight PPS oligomers (Figure 1), agreeing with the

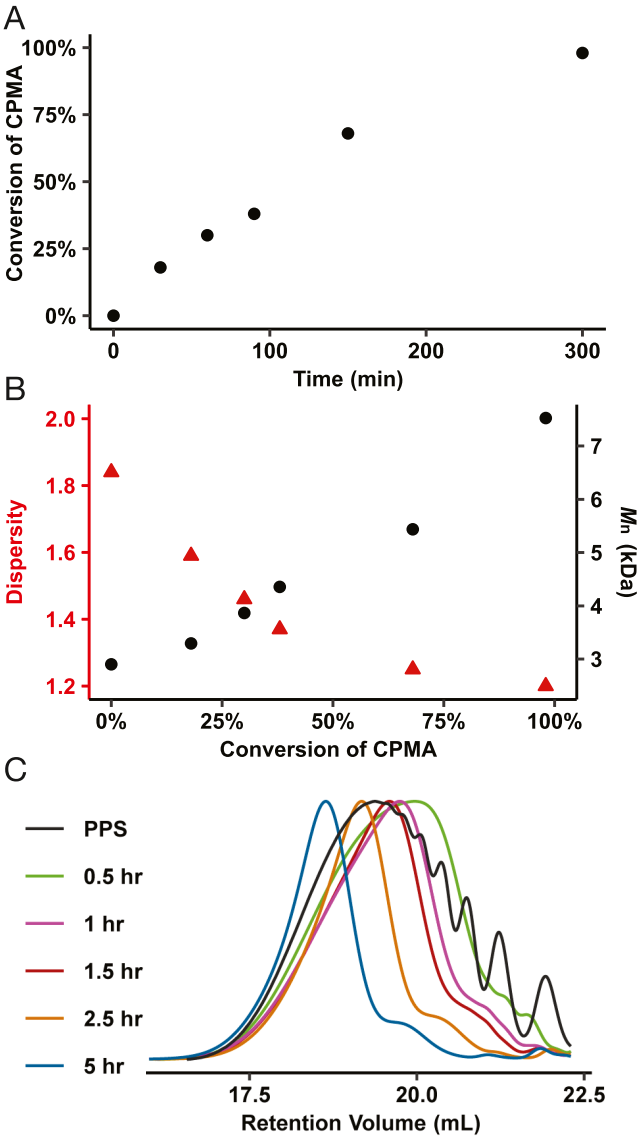

Figure 1. Kinetics of the synthesis of the BC1 prepolymer with 18 wt % PPS. (A, B) Progression of conversion of CPMA (determined by ^{1}H NMR), $Đ$, and M_n during the reaction. (C) GPC traces of aliquots throughout the synthesis showing $Đ$ decreasing and molecular weights increasing.

molecular weight distribution of other condensation polymers that our group has synthesized. We confirmed melt condensation's lack of end-group control by observing three species in decreasing abundance via matrix-assisted laser desorption ionization-time-of-flight mass spectroscopy (MALDI-TOF MS): α-COOH-ω-COOH-PPS, α-OH-ω-COOH-PPS, and α-OH-ω-OH-PPS (Figure S7). Because previous research has shown that COOH and OH initiate ROCOP in similar manners,[36] PPS is represented as having COOH end groups for simplicity (Scheme 1).

Catalyst Choice. We originally intended to use a recently developed bifunctional aminocyclopropenium aluminum catalyst abbreviated as **AlCl**[20,36] because the practical use of ROCOP catalyzed by widely used metal catalysts has only been sparingly explored.[39] Unlike the Et_3B/[PPN]Cl binary system where the Lewis acid and Lewis base are distinct molecules, **AlCl** contains covalently tethered Lewis acid and Lewis base that maintain catalyst activity in diluted polymerization medium and prevent inhibition by protic CTAs.[20,23,36] We initially deemed **AlCl** to be suitable because we wanted to incorporate high-weight percentages of PPS in the block copolymer. While **AlCl** produced the BC1 prepolymer, an ABA triblock copolyester comprising poly(PO-*alt*-CPMA)-*b*-PPS-*b*-poly(CPMA-*alt*-PO) with 10 wt % of PPS (M_n = 8.9 kDa, $Đ$ = 1.14) and 18 wt % of PPS (M_n = 5.4 kDa, $Đ$ = 1.22), the residual catalyst was extremely difficult to remove despite many attempts. Moreover, **AlCl** triggered thiol−ene cross-linking in ten min without UV exposure, rendering it unusable as a photoresin. Cobalt-salen complexes have been used as a photoinitiator for the living radical polymerization of acryloyl and vinyl monomers.[40−42] This reaction occurs under visible light in ambient temperature, and the addition of TPO vastly improves its efficiency.[40,41] **AlCl** might have triggered the premature cross-linking via a similar mechanism.

Further, the brightly colored **AlCl** stained the polymers such that they would interfere with microscopic analysis, which is critical for organ-on-a-chip. Additionally, the use of metals such as Al, Co, and Cr severely limits metal-catalyzed ROCOP's applications in food packaging and medicine.[20,43] The recent advent of boron-based Lewis-pair-catalyzed ROCOP alleviates the toxicity concern and has demonstrated potential in drug delivery and biological imaging.[44] To produce colorless and stable photopolymers, we used an Et_3B/[PPN]Cl bicomponent catalyst system. The resultant BC1 prepolymer with 18 wt % of PPS (entry 1, Table 1) has a higher molecular weight than that produced by **AlCl**. As most reported CTAs are either small molecules or well-characterized polymers with

Table 1. BC1 Prepolymer Synthesized by ROCOP

entry[a]	PPS wt %[b]	[CPMA]/[PO]/[PPS]/[Et_3B]/[[PPN]Cl][c]	M_n (kDa)[d]	$Đ$[d]	T_g (°C)[e]	T_m/T_c (°C)[e]
1	100%	N/A	2.9	1.84	N/A	52/28
2	61%	100:600:12:1:1	3.2	1.54	−23	49/17
3	50%	100:600:7.6:1:1	4.0	1.44	−43	44/−2
4	37%	100:600:4.5:1:1	5.0	1.40	−35	39/NA
5	31%	100:600:3.2:1:1	5.4	1.30	−14	NA
6	18%	100:600:1.6:1:1	7.2	1.24	21	NA

[a]PPS and BC1 prepolymer were synthesized according to Scheme 1. The number in all subscripts represents the weight percentage of PPS (M_n = 2.9 kDa, $Đ$ = 1.84) relative to ring-opened CPMA and PO at full CPMA conversion. [b]Conversion was equivalent to the percentage of ring-opened CPMA and was determined by ^{1}H NMR at the 19th hour of polymerization—all entries reached 100% conversion except for entry 2 (61 wt % PPS), which reached 88% conversion. [c]Small-scale reactions were set up with 3 mmol of CPMA. [d]Determined by GPC in tetrahydrofuran. All molecular weights are apparent molecular weights calibrated with polystyrene standards. [e]Glass transition temperature (T_g), melting temperature (T_m), and crystallization temperature (T_c) were measured by dynamic scanning calorimetry (DSC).

https://doi.org/10.1021/acsapm.3c02745
ACS Appl. Polym. Mater. XXXX, XXX, XXX−XXX

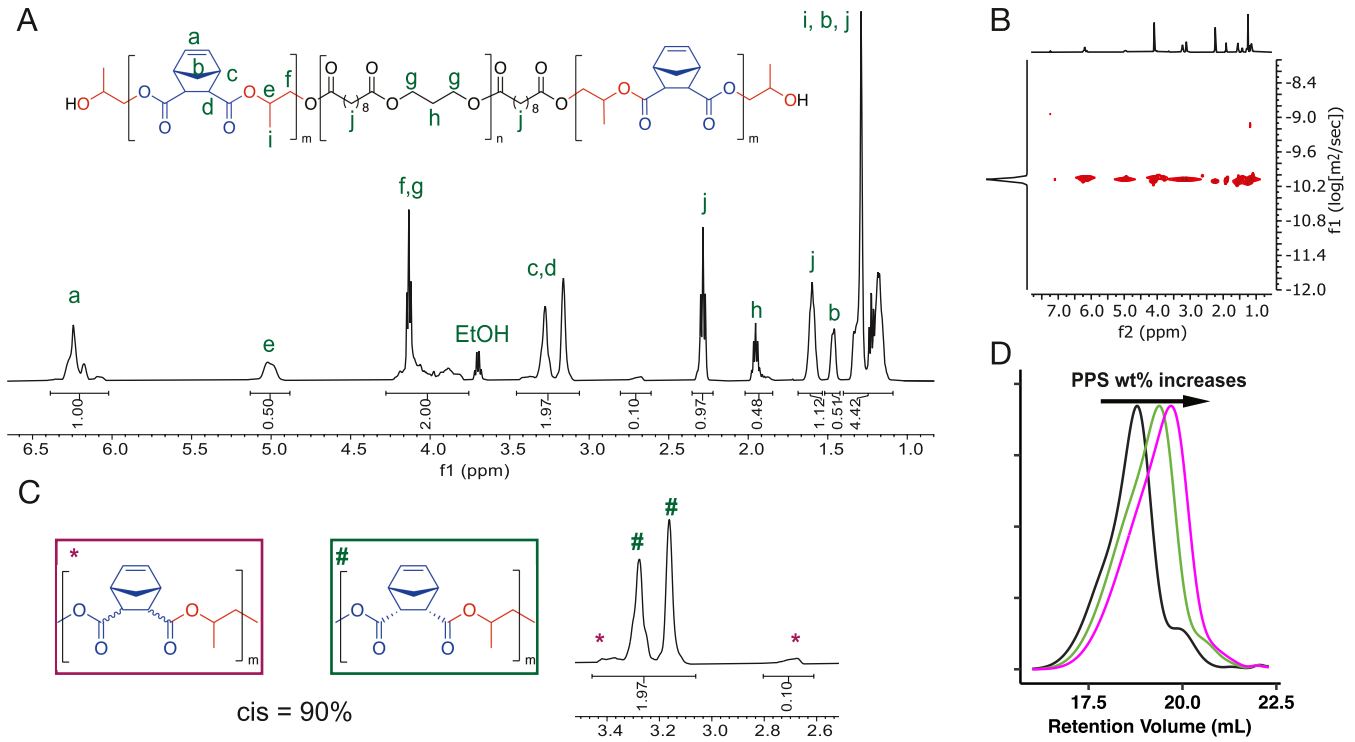

Figure 2. NMR ($CDCl_3$, 500 MHz) and GPC analyses of the BC1 prepolymer. (A) ^1H NMR of the BC1 prepolymer with 31 wt % PPS synthesized on a 30 g scale; (B) diffusion NMR of the previous sample showing all proton signals with the same diffusion coefficient (two peaks with higher diffusion coefficients are from solvents); (C) stereochemistry analysis of the BC1 prepolymer; and (D) GPC traces of the BC1 prepolymer synthesized with various PPS concentrations (entry 4−6, Table 1).

low dispersity,[36] we investigated the chain transfer effect of broadly dispersed PPS.

PPS-Mediated ROCOP is a Controlled Polymerization. We used the 18 wt % PPS to run the kinetic model study. The dependence of M_n and dispersity on PPS equivalence is consistent with the immortal nature of the polymerization. M_n negatively correlates to PPS equivalents (Table 1), confirming that PPS undergoes efficient chain transfer to afford the BC1 prepolymer. In agreement with previous reports of Et_3B/[PPN]Cl catalyzed ROCOP with or without small-molecule CTAs, M_n increases linearly with anhydride conversion and time (Figure 1A,B), validating PPS's linear and uniform chain extension.[21,44] The conversion-M_n best-fit curve intercepts the *y*-axis at 2323 g/mol, approximating the M_n of PPS and suggesting negligible epoxide homopolymerization (Figure 1A). GPC traces of polymerization aliquots have an unimodal distribution, with the series of peaks corresponding to low molecular weight PPS oligomer no longer visible. This suggests that the ring-opened PO rapidly transferred its reactivity to PPS and enabled chain extension. The low molecular weight shoulder likely arises from a poly(PO-*alt*-CPMA) "single block" initiated by chloride from [PPN]Cl (Figure 1C).

Similar to other reported protic CTAs used in ROCOP catalyzed by a bicomponent catalyst,[45] high PPS loadings decrease polymerization rates: polymerization with 18 wt % PPS (entry 6, Table 1) reached complete conversion in 5 h, while the one with 61 wt % PPS reached only 88% conversion in 19 h (entry 2, Table 1). High PPS loadings likely inhibit catalyst activity due to increased reaction viscosity, dilution of the active catalytic species, and competition with the binding of the growing anionic chain to the active catalytic species. Notably, the M_n of the BC1 prepolymer is significantly lower than their theoretical M_n calculated via stoichiometry ratios in Table 1. In addition to the polystyrene standards only giving a relative molecule weight, low molecular weight PPS species (Figure 1C) and potential side products, such as cyclic macromers resulting from backbiting or anhydrides from the condensation of two sebacic acids, may result in inaccurate calculation of the PPS concentration. In contrast, small-molecule CTAs and polymeric CTAs with low dispersity ($Đ$ < 1.1) can achieve good agreement between the experimental and theoretical M_n because they have well-defined structures and discrete molecular weights, enabling precise calculation of their concentrations.[36] The high dispersity ($Đ$ = 1.82) and ill-defined structures of PPS make it difficult to calculate its molar concentration to study the exact inhibition mechanism.[36]

Characterization of the BC1 Prepolymer. The absence of ether linkages—evidenced by the absence of polyether signals on ^1H NMR (δ = 3.5−3.7 ppm)—indicates that only alternating copolymerization of CPMA and PO occurred (Table 1 and Figures 2A and S1−S5). Scaling up the reaction from small-scale kinetic studies to a 30 g scale did not decrease monomer conversion, neither did it broaden the dispersity. Nevertheless, weighing [PPN]Cl crystals directly to the reaction mixture caused noticeable polyether formation and low anhydride conversion at high PPS concentrations (50 and 61 wt %), likely due to a higher likelihood of inexact ratios of Et_3B relative to [PPN]Cl/PO homopolymerization suggests a larger fraction of PO was being activated by a slight excess of Et_3B.[46−50] At larger excess, Chidara et al.[46] reported the formation of polyether-rich products that possess very different properties and are resistant to hydrolytic degradation. It is, therefore, imperative to keep the Et_3B-[PPN]Cl ratio exact by using the stock solution. On the flip side, while excess [PPN]

https://doi.org/10.1021/acsapm.3c02745
ACS Appl. Polym. Mater. XXXX, XXX, XXX−XXX

Cl does not trigger such a side reaction, its basicity may promote transesterification during ROCOP. Stereochemistry analysis with the ^{1}H NMR spectrum shows that 10% of ring-opened CPMA adopt a trans-conformation, and varying concentrations of PPS have no effect on the stereoselectivity (Figure 2C). Prolonged incubation in excess PO is likely the major contributor to the observed stereoirregularity, which is caused by epimerization of the cis CPMA ester linkages in the poly(PO-*alt*-CPMA) backbone.[51] Diffusion NMR shows a unimodal distribution of diffusion coefficients, suggesting that the PPS and poly(PO-*alt*-CPMA) are in the same backbone (Figure 2B). MALDI-TOF mass spectroscopy of the BC1 prepolymer with 50 and 61 wt % of PPS (entries 2 and 3, Table 1) confirms its ABA triblock architecture furnishing uniform propanol chain ends with a distribution of block lengths (Figure 3). The observed mass values account for all

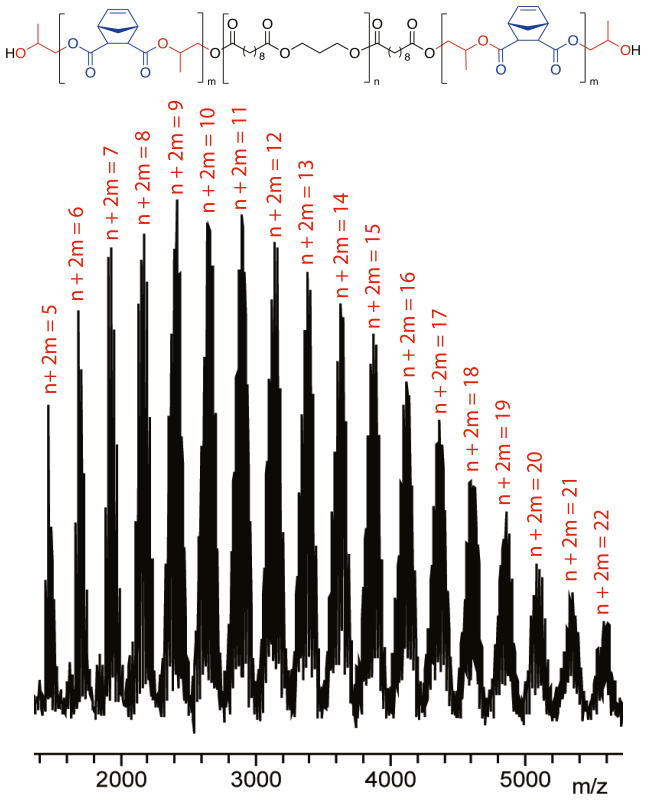

Figure 3. MALDI-TOF of the BC1 prepolymer with 61 wt % PPS. Only chains initiated from α-COOH-ω-COOH-PPS are labeled for simplicity, although observed mass values also account for the triblock copolyester initiated from α-OH-ω-OH-PPS or α-COOH-ω-OH-PPS (Figure S9).

three possible microstructures that resulted from three different end-group combinations of PPS (Figures S8−S10). The Gaussian distribution within each cluster indicates a statistical distribution of different numbers of sebacate-propanediol units and CPMA-PO units (Figure S9). We attribute 2417 m/z to three possible species: [α-OH-ω-COOH-(PPS)$_4$]-*block*-(PO-*alt*-CPMA)$_6$, [α-OH-ω-OH-(PPS)$_4$]-block-(PO-*alt*-CPMA)$_6$, and [α-COOH-ω-COOH-(PPS)$_3$]-block-(PO-*alt*-CPMA)$_6$ (Figure S9 and Table S1). The identification of 2438 m/z validates our tabulated analysis (Table S2). We did not observe any polyether segment or chloride-initiated chain because they could not afford the observed mass patterns.

A high catalyst loading (18 wt % PPS, entry 6, Table 1) leads to chloride-initiated chains that manifest as a low molecular weight shoulder (Figures 1C and2D) on the GPC chromatogram. In addition, MALDI-TOF of the crude reaction mixture quenched at low conversion revealed both chloride-initiated chains and PPS-initiated chains (Figure S11). So does the diffusion NMR of entry 6, Table 1 at full conversion, revealing two polymeric species with disparate diffusion coefficients (Figure S6). In contrast, a higher PPS loading minimizes the probability of the chloride-initiated species chain extending to any significant degree: GPC chromatograms of entry 5, Table 1 (31 wt % PPS), and entry 4, Table 1 (37 wt % PPS), do not contain any low molecular weight shoulder (Figure 2D)—and diffusion NMR of entry 5, Table 1 (31 wt % PPS), displays a unimodal distribution of diffusion coefficients (Figure 1B).

The dispersity of the BC1 prepolymer is lower than that of PPS and decreases as the PPS equivalent increases (Table 1). The dispersity similarly decreased (Figure 1C) during the polymerization of entry 6, Table 1 (18 wt % PPS). In ROCOP conducted with small-molecule CTAs, dispersity is generally invariant with the degree of polymerization, and a low dispersity is maintained due to rapid equilibration between anionic chain ends and protic species. Further, the few examples of ROCOP conducted with macroCTAs used commercially available polymers with low dispersity.[23,36] We, therefore, surmised that this downward trend of dispersity stemmed from a diffusion-controlled chain transfer mechanism. Low molecular weight fractions of PPS likely chain-extend more rapidly. This mechanism preferentially decreases the abundance of low molecular weight species, subsequently decreasing the dispersity. Indeed, the progression of molecular weight with time (Figure 1) for entry 6, Table 1 (18 wt % PPS), showed that low molecular weight PPS oligomers were consumed within 30 min. Lastly, PPS is absent in MALDI-TOF of entry 6, Table 1 (18 wt % PPS), quenched in 30 min, corroborating with the observation that PPS is an efficient CTA.

This synthesis strategy bridges the dichotomy between ROCOP and polycondensation, providing access to polyesters that cannot be synthesized via either method alone. Notwithstanding its broad substrate scope, ROCOP requires cyclic anhydrides. Yet cyclic anhydrides of many biologically relevant diacids like ketoglutaric acid, sebacic acid, and azelaic acid, either are not commercially available or difficult to synthesize.[29] Furthermore, for biologically relevant diacids with commercially available anhydrides (such as succinic anhydride, glutaric anhydride, tartaric anhydride, and itaconic anhydride), they are either too sluggish to react or, in the case of itaconic anhydride, have acidic protons that are incompatible with the growing alkoxide chain ends during the ROCOP process. On the other hand, polycondensation can incorporate these diacids, but its harsh reaction condition often causes degradation or premature cross-linking of reactive functional groups, which manifests as large dispersity ($Đ$ = 1.7−10) and batch-to-batch inconsistencies.[52,53] Sebacate-derived elastomers, especially PGS, are therefore still commonly functionalized by reacting its pedant secondary alcohol groups with acyl chlorides, anhydrides, or carbodiimides, all of which need a large amount of hazardous reagents.[37,54−56] Therefore, metal-free ROCOP and polycondensation complement each other in producing functional polyesters.

https://doi.org/10.1021/acsapm.3c02745
ACS Appl. Polym. Mater. XXXX, XXX, XXX−XXX

Thermal and Mechanical Properties of Block Copolyesters with Various PPS Content. We used DSC and thermogravimetric analysis (TGA) to probe the thermal behaviors of the BC1 prepolymer and the cured BC1 resin. While alternating polyesters comprising PO and tricyclic anhydrides have high T_g (above 70 °C) but no T_m,[45,49] the octylmethylene segment of PPS confers flexibility and lowers the T_g of the BC1 prepolymer. All polymer samples' T_g is lower than 37 °C and negatively correlates to equivalents of PPS—despite leftover CPMA likely making entry 2, Table 1 (61 wt % PPS), an outlier—its T_g reverts the downward trend and is 20 °C higher than that of entry 3, Table 1 (50 wt % PPS, T_g = −43 °C). At higher equivalents of PPS (entry 2−4, Table 1), the BC1 prepolymer adopts more PPS characters by displaying distinctive T_m and T_c (PPS: T_m = 52 °C, T_c = 28 °C): T_m increases from 39 °C (entry 4, Table 1, 37 wt % PPS) to 49 °C (entry 2, Table 1, 61 wt % PPS) and T_c increases from −2 °C (entry 3, Table 1, 50 wt % PPS) to 17 °C (entry 2, Table 1, 61 wt % PPS). We attributed the lack of T_c of block copolymers with lower PPS concentration to their decreased chain mobility due to the rigid norbornene backbone. At higher concentrations of PPS, the slight increase in the PPS fraction within the block copolymer has a much higher impact on polymers' T_c. Overall, T_m and T_c differ by a lot for most of the samples; this is because PPS and poly(CPMA-*alt*-PO) blocks each have very distinctive properties. The sebacate-derived polyester with a similar structure typically has very low T_g and T_m and absent T_c due to its very flexible octylmethylene chain.[52,53,55,57] But poly(CPMA-*alt*-PO) is the contrary: the rigid bicyclic ring of CPMA significantly limits the chain's degree of freedom.

Due to the reactivity of norbornene, increasing the length of the poly(PO-*alt*-CPMA) block renders BC1 prepolymer less stable at high temperatures. Entry 3, Table 1 (50 wt % PPS), shows a two-step degradation with the first onset at 223 °C and the second onset at 376 °C (Figure S19), and PPS has a single onset at 377 °C (Figure S18). We attributed the first onset of entry 3, Table 1 (50 wt % PPS), to the poly(PO-*alt*-CPMA) block. In addition to a similar stepwise degradation in entry 2, Table 1 (61 wt % PPS), we also identified a minor transition at 151 °C and attributed it to leftover CPMA (Figure S20). As the first degradation was not complete when the second degradation took place, we could not derive the weight percentage of each block from TGA data.

Norbornene-functionalized polymers have been explored in 3D printing because of their facile thiol−ene cross-linking.[4,10,11] We chose PETMP as the cross-linker due to its applications in denture materials, low vapor pressure, and efficient generation of highly cross-linked thiol−ene networks.[58−60] The BC1 prepolymer cross-linked rapidly with PETMP in the presence of TPO, a photoinitiator, when exposed to 385 nm ultraviolet light during the photorheology experiment (Figure 4A). The resultant network was elastomeric and underwent cyclic loading and unloading (0−12% strain range) 50 times without breakage (Figure 4B). Furthermore, cycles 1, 25, and 50 exhibited nearly identical elastic behavior with very small hysteresis (Figure 4B). The block copolymer design interrupted the otherwise dense and rigid thiol−ene network with the uncross-linked PPS block. As expected, the increasing length of the PPS block decreased the cross-linking density and, therefore, Young's modulus (Figure 4F). The ultimate strain correspondingly increased from ϵ_{max} = 22 ± 0.3% for the BC1 prepolymer with 25 wt % PPS to ϵ_{max} = 58 ± 4% for the block copolyester with 31 wt % PPS, although

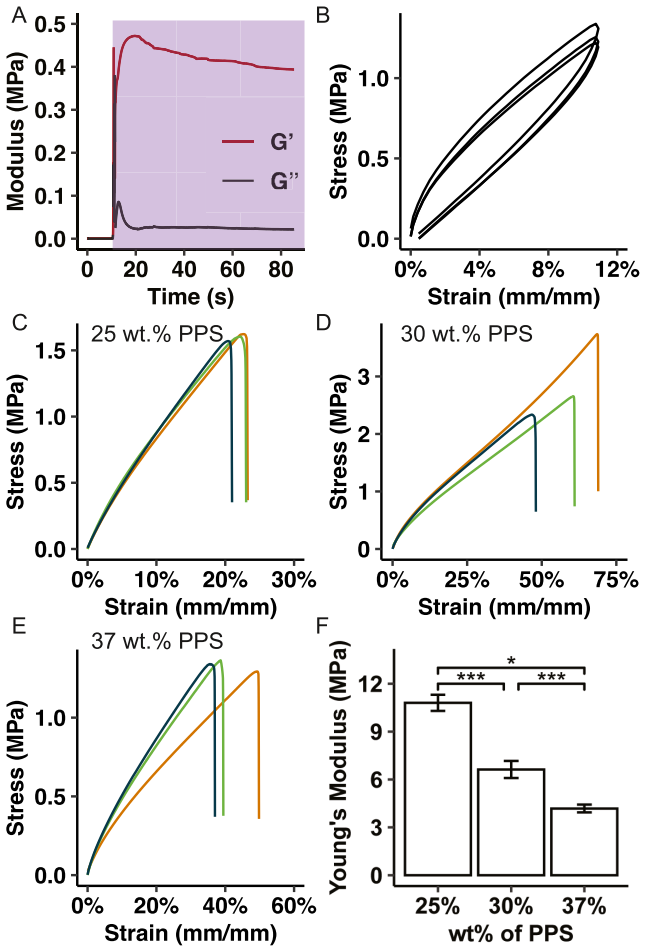

Figure 4. Mechanical testing of the BC1 prepolymer cross-linked with PETMP. (A) Photocuring kinetics of entry 6, Table 1 cured by PETMP with TPO as the initiator; magenta box represents the onset of UV exposure (385 nm, 3 W). (B) Cyclic tensile testing of cured entry 6, Table 1 (18 wt % PPS) showing traces of cycle 1, cycle 25, and cycle 50. (C−E) Tensile testing of various polymer samples (n = 3). (F) Comparison of Young's modulus derived from tensile testing. *p < 0.05 ***p < 0.001.

the one with 37 wt % PPS showed no significant difference to either (Figure 4C−E). It is important to note that the BC1 prepolymer used for mechanical testing was made from another batch of PPS with molecular weights and dispersity different from those of PPS used for the kinetic study. Notwithstanding batch-to-batch variations of PPS, these results confirmed that our polymerization strategy allowed us to tune the mechanical properties by varying block lengths, a level of control that is difficult to achieve with step-growth polycondensation. Taken together, BC1 prepolymer contrasts a class of recently reported photopolymers from ROCOP of CPMA and limonene oxide,[19] which is relatively stiff, with a high Young's modulus and low strain at failure. We attribute BC1's elasticity and flexibility to its network structure, where the densely cross-linked poly(CPMA-*alt*-PO) blocks are interrupted by the long, flexible PPS block. Using reactive diluent, as the one shown in Figure 5, can further reduce cross-linking density and increase BC1's flexibility.

3D Printing of the BC1 Resin. We investigated the printability of the BC1 prepolymer with 31 and 37 wt % of PPS because they did not contain a significant fraction of chloride-initiated chains. Notably, the one with 31 wt % of PPS

https://doi.org/10.1021/acsapm.3c02745
ACS Appl. Polym. Mater. XXXX, XXX, XXX−XXX

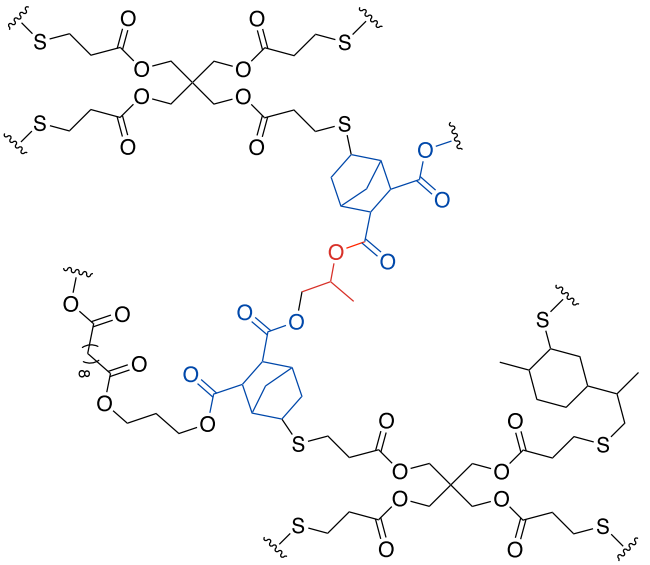

Figure 5. Structure of photo-cross-linked BC1 with limonene as the reactive diluent. 1 wt % of TPO and 0.5 wt % of UV stabilizer, butylated hydroxytoluene (BHT), were used to formulate the BC1 resin. The resin was cured under UV LED (385 nm, 30 mW/cm^2) in five to ten seconds. The wavy line represents the remainder of the cross-linked network.

synthesized on a 30 g scale had higher molecular weights (M_n = 8.2 kDa) and lower dispersity ($Đ$ = 1.20) than its small-scale equivalent (entry 5, Table 1). This improvement in polymerization performance likely results from the Schlenk bomb's superior air-free environment compared to that of vials, as well as the more accurate addition of Et_3B and [PPN]Cl at a large scale. The BC1 prepolymer's high viscosity requires proper diluents. Inert diluents such as propylene carbonate, ethyl acetate, and acetone caused poor *xy* resolution and significant shrinkage stress during solvent removal. Reactive diluents, on the other hand, first serve as a plasticizer to reduce the viscosity and covalently integrate with the cross-linked network during curing, therefore causing very little shrinkage stress during washing. We investigated diethyl fumarate and limonene. Diethyl fumarate afforded a printable resin (E = 3.49 ± 0.23 MPa, ϵ_{max} = 73 ± 5%), but limonene is more interesting: it is renewably sourced, relatively safe for human consumption, and has been used in DLP resins with good printability and cytocompatibility.[61]

We formulated printable BC1 resin using the BC1 prepolymer with 31 wt % PPS, limonene, and PETMP. BC1 is transparent and clear, similar to poly(dimethylsiloxane) (PDMS) (Figure 6A), the staple polymer used to manufacture microfluidics and other biomedical implants.[7,62] Five-second exposure per layer consistently produced good resolutions, whereas underexposure or overexposure caused layer detachment or low *xy* resolutions. Prints of various structural complexity demonstrate the versatility of BC1 (Figure 6A, left). In particular, the 3D-printed culture wells (Figure 6A, center) suggest the resin had enough mechanical strength to withstand the suction force created when the newly formed layer detach from the resin vat.[8,63] Despite the optimized formulation and printing parameters, the BC1 prepolymer with 37 wt % PPS cracked promptly during washing with organic solvents. We deduce that with a longer PPS block length reducing the cross-linking density, the resultant materials cannot withstand the swelling-induced mechanical stress. To further demonstrate BC1's performance, we printed a flow device with Y-shaped enclosed channels and used food dyes to showcase their patency (Figure 6A, right). Adding more roof layers would eventually clog the channel with residual resin, but we believe adding photo absorbers to BC1 will limit the cure depth and prevent overcuring.

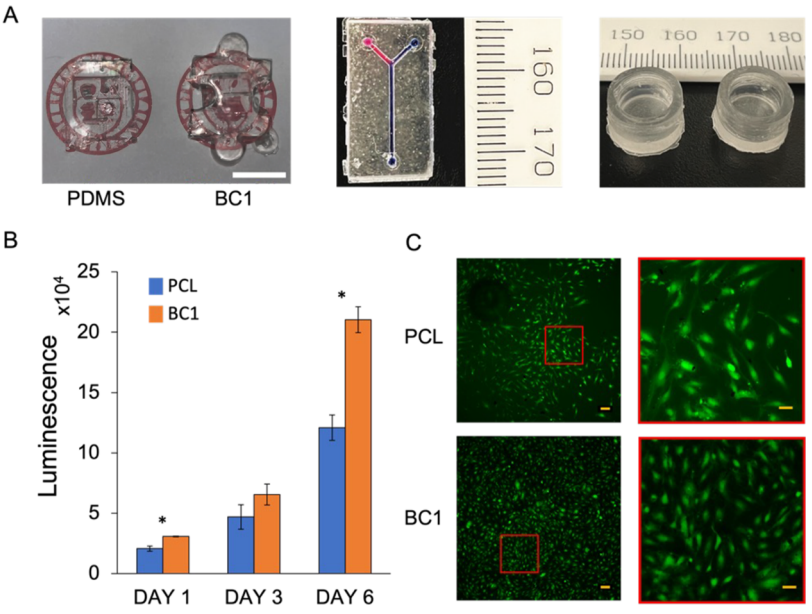

Figure 6. 3D Printing and cytocompatibility of BC1 with 31 wt % PPS (M_n = 8.2 kDa, $Đ$ = 1.20). (A). Left: Comparison between PDMS and BC1 (scale bar: 1 cm; background logos are blurred due to journal copyright requirements); center: a 3D-printed microfluidic device with Y-shaped channels (1 mm diameter); right: 3D printed cell culture wells. (B) *In vitro* viability of HUVECs cultured on BC1 or PCL; luminescence signal linearly correlates to the number of viable cells (*p < 0.05). (C) Calcein-AM staining of HUVECs cultured on BC1 and PCL films (scale bar: 100 μm).

https://doi.org/10.1021/acsapm.3c02745
ACS Appl. Polym. Mater. XXXX, XXX, XXX−XXX

Ene-thiol ratio	Young's Modulus (MPa)	Strain at Break (mm/mm)	UTS (MPa)
2:1	4.23 ± 0.48	43% ± 5%	1.37 ± 0.02
1:1	9.82 ± 0.62	36% ± 9%	1.87 ± 0.11

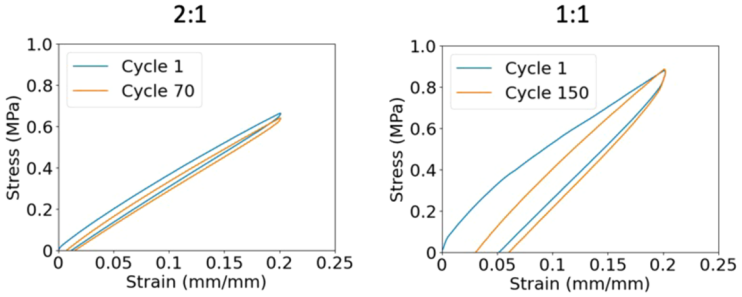

Figure 7. Thiol stoichiometry affects BC1's mechanical properties. UTS: Ultimate tensile stress.

To determine the cytocompatibility of BC1, we seeded adherent HUVECs on 2D films of cured BC1 resin PCL (a polyester with well-documented biocompatibility and established applications in medicine). We measured the cellular metabolic activity with an ATP luminescence assay to reflect the cell viability over 6 days. Not only did we not observe any cytotoxic effect of the BC1 resin compared to PCL, but we also saw higher HUVEC viability on days 1 and 6 with BC1. Particularly on day 6, HUVECs cultured on BC1 showed almost double the viability than those cultured on PCL (Figure 6B). Visual inspection of calcein-AM staining images taken on day 6 confirmed HUVECs' higher density on the BC1 surface (Figure 6C). HUVECs cultured on both surfaces maintained their characteristic cobblestone morphology throughout the test period (Figures 6C and S21). BC1's more hydrophilic surface, arising from hydrophilic monomers (1,3-propanediol and PO) and thiol-ether linkages, may promote better cell adhesion and proliferation.[64] Although residual catalysts were never fully removed from the polymer, they did not exert observable cytotoxicity, corroborating with Luo et al.'s findings that the unremoved Et_3B-phosphazene catalyst pair is not cytotoxic toward the CCK-8 fibroblast.[65]

Optimizing BC1 for printing microfluidics with more complex channels will be a herculean undertaking that takes many iterations. Only certain commercial resins and low molecular weight poly(ethylene glycol) diacrylate have been successful. External factors such as printing settings, resin age, resin viscosity, and even humidity can affect the degree of curing and thus the concentration of uncured monomers/oligomers that can leach into their surroundings, thereby further complicating the development of biocompatible resins.[8]

After evaluating the performance of BC1, we probed how an off-stoichiometry formulation would impact its properties. Ostemer by Mercene Lab uses this strategy, which researchers employ to fabricate organ-on-a-chip devices with chemically active surfaces.[7] When we halved the amount of PETMP, the resultant off-stoichiometry BC1 remained printable, with Young's modulus correspondingly decreasing due to a lower cross-linking density (Figure 7). Naturally, more unreacted alkenes are present on the surface of off-stoichiometry BC1 according to infrared spectroscopy (Figure S22). This results in a much smaller hysteresis during elastic recoil, and it ruptured earlier during cyclic testing (Figure 7). Future work will conduct thiol−ene surface modification with functional molecules, be that cysteine-containing cell adhesive peptides or other signaling molecules, to improve cell adhesion or elicit certain cellular responses.

CONCLUSIONS

This report bridges the dichotomy between polycondensation and ROCOP to afford polyester-based thiol−ene resins with good promise in biomedical applications. The significance of our work is two-pronged. First, the Et_3B-assisted ROCOP of cyclic anhydride and epoxide—in conjunction with melt condensation—can be scaled up to 30 g while maintaining good control over end-group identity and dispersity. Polycondensation working in tandem with ROCOP will readily accelerate the discovery of new materials without the invention of new catalysts, monomers, or polymerization methodologies. Second, ABA triblock copolyesters can be a photopolymer for 3D printing of materials with desirable properties; ROCOP's compatibility with CTAs of vastly different structures, as well as monomers of diverse functionalities, help to meet the increasing demand for 3D-printed biomaterials with tailored properties and facile functionalization.

EXPERIMENTAL SECTION

Materials. All chemicals were purchased from commercial sources and used without purification unless noted otherwise. PO was stirred over calcium hydride for 3 days and then vacuum transferred to a Straus flask for long-term storage in the glove box. CPMA was purified under vacuum sublimation at 70 °C. [PPN]Cl was recrystallized by layering diethyl ether over a saturated solution of [PPN]Cl in dichloromethane (DCM).

Synthesis of PPS. A single-neck round-bottom flask was charged with a stir bar, 1.05 equiv of sebacic acid, and 1.0 equiv of 1,3-propanediol. A distillation tube with a 0−4 Hi-vac valve was then attached to the flask, and a receiving flask was connected to the other end. The assembled reaction apparatus was evacuated and refilled with nitrogen three times to remove oxygen and moisture. Afterward, it was put under a constant flow of nitrogen, first reacting under nitrogen at 160 °C for three h and then at 210 °C for 2 h.

ROCOP of CPMA and PO. To conduct small-scale ROCOP, CPMA and appropriate amounts of catalysts (see Table 1) were added into a dram vial with a stir bar in the glove box, followed by adding PO with a syringe. The reaction mixtures were sealed with a Teflon cap that was further secured with electrical tapes. Vials were taken outside to stir at 60 °C for the desired amount of time. Large-

https://doi.org/10.1021/acsapm.3c02745
ACS Appl. Polym. Mater. XXXX, XXX, XXX−XXX

scale ROCOP followed a similar procedure but was conducted in Schlenk bomb tubes sealed with Kontes valves. Conversions were calculated by integration of corresponding peaks in the ^{1}H NMR spectrum of reaction crude. Polymers were purified by precipitating in a 1:1 water/ethanol mixture and subsequently dried under a high vacuum overnight. ^{1}H NMR spectra of purified samples (Figures S1−S7) were then recorded to analyze if homopolymerization of PO occurred.

Polymer Characterization. NMR spectra were recorded on a Bruker AV III HD, 500 MHz spectrometer with a broadband Prodigy cryoprobe or Varian IVarian INOVA 400, 400 MHz spectrometer. $CDCl_3$ was used as the NMR solvent. MALDI-TOF-MS analysis was performed on a Bruker AutoFlex Max MALDI-TOF Mass Spectrometer in linear mode. MALDI matrix was 2-[(2*E*)-3-(4-*tert*-Butylphenyl)-2-methylprop-2-enylidene]malononitrile (DCTB) and potassium trifluoroacetate (KTFA) was the ionizing agent. To prepare MALDI samples, 50 μL of polymer solution (1 mg/mL in THF) was mixed with 100 μL of KTFA solution (5 mg/mL in THF) and 400 μL of DCTB solution (40 mg/mL in THF); this formula gave the best to signal-to-noise ratio. The sample solutions were then blotted to the target plate with capillary tubes and allowed to air-dry for 15 min before MALDI analysis. The resultant mass spectra were processed and analyzed with a Bruker Autoflex in linear mode. GPC was conducted using the Malvern Panalytical OMNISEC GPC system (Malvern Instruments Ltd., Malvern, U.K.) via a refractive index detector and a column set of T6000 M and T3000 with THF as the mobile phase (1 mL/min flow rate). The polymers were dissolved in HPLC grade THF at 5.0 mg/mL and filtered through a PTFE syringe filter. M_n, M_w, and $Đ$ were determined according to polystyrene standards. DSC was conducted on a TA Instruments Q1000 Modulated Differential Scanning Calorimeter to determine the glass transition temperature T_g, T_m, and T_c.

Preparation of Cross-Linked Samples. To prepare cross-linked block copolyesters for mechanical and thermal testing, a polymer solution in propylene carbonate was spread in a mold and UV-cured by a hand-held UV lamp (365 nm) for one min with PETMP in the presence of TPO. Propylene carbonate was removed via sequential washing in ethanol with 75, 50, and 25% propylene carbonate and eventually pure ethanol. Residual ethanol was then removed in vacuo. Tensile testing bars were then cut out with a die. Tensile testing and cyclic testing were conducted at room temperature on an Instron 5943 equipped with a 50 N loading cell and Bluehill Universal software. To prepare samples for photorheology, a solution was prepared similarly to the above. Photorheology was conducted at room temperature on a TA Instruments DHR3 Rheometer equipped with a UV curing accessory; the geometry was a 20 mm parallel plate composed of a disposable aluminum upper plate and an acrylic lower plate. A 365 nm UV filter was used, and the power output was 30 mW.

Resin Preparation and 3D Printing. For a large-scale ROCOP, 9.11 g of PPS, 15.1 g of CPMA, and 36 mL of PO were added to a Schlenk bomb flask in a nitrogen-filled glove box. [PPN]Cl (1 M in DCM) and triethylborane (1 M in hexane), 0.92 mL each, were added to the mixture. The bomb flask was then sealed and taken outside to stir at 60 °C for 19 h. The reaction was quenched with a small amount of ethanol and then mixed with 20 mL of limonene. BHT and TPO, 675 mg each, were dissolved together in 5 mL of acetone, and the solution was added to the resin mixture. The mixture was then stirred in the open air away from light to reach homogeneity. If PO was evaporated *in vacuo*, a proper amount of polar solvents such as ethyl acetate and acetone should be added to lower the viscosity. Lastly, PETMP was added to the mixture, which was then stirred briefly to acquire a homogeneous and viscous solution. 3D printing was conducted on an Asiga Max 3D printer equipped with a 385 nm light source and each layer was printed with a five s exposure and at 30 mW/cm^2. For postprocessing, printed objects were briefly washed with acetone, followed by an extensive wash in 2-propanol to remove uncured resins, and then postcured in the Asiga Flash UV chamber.

Cytocompatibility Study. To prepare thin films for the cytocompatibility study, 6 mm glass coverslips were briefly dipped in 1 wt % solution PCL (in chloroform) or BC1 (in acetone). After air-drying, the coverslips were incubated under ultraviolet light (Asiga Flash UV Curing Chamber) for 30 min. They were then placed in 24-well plates and washed sequentially with 100% ethanol, 75% ethanol in water, and water for 20 min per wash. The *in vitro* cytocompatibility of the films was performed using human umbilical vein endothelial cells (HUVEC, C2519A, Lonza, MD). HUVEC (passages 4−6) were cultured using an endothelial cell growth medium MV 2 kit that contained 5% fetal bovine serum and supplements (C-22121, PromoCell/VWR, PA). The cells were harvested using trypsin-EDTA after reaching confluency, neutralized with medium, centrifuged at 200g for 5 min, and resuspended to obtain 10^4 cells/mL. 50 μL of the suspension (500 cells/50 μL) was added dropwise onto the coverslips, and the cells were incubated for 3 h before 1 mL of the medium was added to each well. Cells were incubated at 37 °C with 100% humidity and 5% CO_2. The medium was exchanged every 48 h. A Cell Titer Glo 2.0 assay kit (G9241, Promega, WI) was used to measure the luminescence of the amount of ATP present, which indicated the presence of metabolically active cells after 1, 3, and 6 days. The luminescence (relative light units (RLU)) was recorded using a SpectraMax M3 microplate reader (Molecular Devices, CA). Live assays were also performed after 6 days using calcein-AM (C3100MP, Invitrogen, NY). Live cells were identified when calcein-AM in medium (1 μM final concentration) was converted to green fluorescence after interacting with intracellular esterases. The fluorescent images were observed by using a Nikon ECLIPSE Ti fluorescence microscope (Nikon Instruments INC., NY).

■ ASSOCIATED CONTENT

Supporting Information

The Supporting Information is available free of charge at https://pubs.acs.org/doi/10.1021/acsapm.3c02745.

^{1}H NMR spectra, MALDI spectra and calculation, and TGA and DSC results (PDF)

■ AUTHOR INFORMATION

Corresponding Author

Yadong Wang − *Meinig School of Biomedical Engineering, College of Engineering, Cornell University, Ithaca, New York 14853-1801, United States;* orcid.org/0000-0003-2067-382X; Email: yw839@cornell.edu

Authors

Warrick Ma − *Department of Chemistry and Chemical Biology, Baker Laboratory, Cornell University, Ithaca, New York 14853-1801, United States; Meinig School of Biomedical Engineering, College of Engineering, Cornell University, Ithaca, New York 14853-1801, United States*

Paula G. Miller − *Meinig School of Biomedical Engineering, College of Engineering, Cornell University, Ithaca, New York 14853-1801, United States*

Complete contact information is available at: https://pubs.acs.org/10.1021/acsapm.3c02745

Notes

The authors declare no competing financial interest.

■ ACKNOWLEDGMENTS

The authors thank Dr. Anthony M. Condo for assistance with MALDI-TOF experiments, Dr. Ivan Keresztes for discussion on diffusion NMR, Karl J. Termini for custom-made glassware, Dr. Andrew Weems for discussion on DLP, and Sarah Severson and Dr. Geoffrey W. Coates their feedback during manuscript preparation. This work made use of the CCMR

Shared Experimental Facilities and the NMR Facility at Cornell University, which are supported by the NSF DMR-1719875 and CHE-1531632, respectively. This work was solely supported by a startup fund from Cornell University. The authors declare no other source of funding.

REFERENCES

(1) Bagheri, A.; Jin, J. Photopolymerization in 3D Printing. *ACS Appl. Polym. Mater.* **2019**, *1*, 593−611.
(2) Bhattacharjee, N.; Urrios, A.; Kang, S.; Folch, A. The upcoming 3D-printing revolution in microfluidics. *Lab Chip* **2016**, *16*, 1720−1742.
(3) Bhattacharjee, N.; Parra-Cabrera, C.; Kim, Y. T.; Kuo, A. P.; Folch, A. Desktop-Stereolithography 3D-Printing of a Poly(dimethylsiloxane)-Based Material with Sylgard-184 Properties. *Adv. Mater.* **2018**, *30*, No. 1800001.
(4) Weems, A. C.; Arno, M. C.; Yu, W.; Huckstepp, R. T. R.; Dove, A. P. 4D polycarbonates via stereolithography as scaffolds for soft tissue repair. *Nat. Commun.* **2021**, *12*, No. 3771.
(5) Merckle, D.; King, O.; Weems, A. C. Ring-Opening Copolymerization of Four-Dimensional Printable Polyesters Using Supramolecular Thiourea/Organocatalysis. *ACS Sustainable Chem. Eng.* **2023**, *11*, 2219−2228.
(6) Kuo, A. P.; Bhattacharjee, N.; Lee, Y.; Castro, K.; Kim, Y. T.; Folch, A. High-Precision Stereolithography of Biomicrofluidic Devices. *Adv. Mater. Technol.* **2019**, *4*, No. 1800395.
(7) Urrios, A.; Parra-Cabrera, C.; Bhattacharjee, N.; Gonzalez-Suarez, A. M.; Rigat-Brugarolas, L. G.; Nallapatti, U.; Samitier, J.; DeForest, C. A.; Posas, F.; Garcia-Cordero, J. L.; Folch, A. 3D-printing of transparent bio-microfluidic devices in PEG-DA. *Lab Chip* **2016**, *16*, 2287−2294.
(8) Musgrove, H. B.; Catterton, M. A.; Pompano, R. R. Applied tutorial for the design and fabrication of biomicrofluidic devices by resin 3D printing. *Anal. Chim. Acta* **2022**, *1209*, No. 339842.
(9) Musgrove, H. B.; Cook, S. R.; Pompano, R. R. Parylene-C Coating Protects Resin-3D-Printed Devices from Material Erosion and Prevents Cytotoxicity toward Primary Cells. *ACS Appl. Bio Mater.* **2023**, *6*, 3079−3083.
(10) Lim, K. S.; Galarraga, J. H.; Cui, X. L.; Lindberg, G. C. J.; Burdick, J. A.; Woodfield, T. B. F. Fundamentals and Applications of Photo-Cross-Linking in Bioprinting. *Chem. Rev.* **2020**, *120*, 10662−10669.
(11) Ooi, H. W.; Mota, C.; ten Cate, A. T.; Calore, A.; Moroni, L.; Baker, M. B. Thiol-Ene Alginate Hydrogels as Versatile Bioinks for Bioprinting. *Biomacromolecules* **2018**, *19*, 3390−3400.
(12) King, O.; Pérez-Madrigal, M. M.; Murphy, E. R.; Hmayed, A. A. R.; Dove, A. P.; Weems, A. C. 4D Printable Salicylic Acid Photopolymers for Sustained Drug Releasing, Shape Memory, Soft Tissue Scaffolds. *Biomacromolecules* **2023**, *24*, 4680−4694.
(13) Cai, Z. Y.; Wan, Y.; Becker, M. L.; Long, Y. Z.; Dean, D. Poly(propylene fumarate)-based materials: Synthesis, functionalization, properties, device fabrication and biomedical applications. *Biomaterials* **2019**, *208*, 45−71.
(14) Luo, Y. Y.; Le Fer, G.; Dean, D.; Becker, M. L. 3D Printing of Poly(propylene fumarate) Oligomers: Evaluation of Resin Viscosity, Printing Characteristics and Mechanical Properties. *Biomacromolecules* **2019**, *20*, 1699−1708.
(15) Kirillova, A.; Yeazel, T. R.; Gall, K.; Becker, M. L. Thiol-Based Three-Dimensional Printing of Fully Degradable Poly(propylene fumarate) Star Polymers. *ACS Appl. Mater. Interfaces* **2022**, *14*, 38436−38447.
(16) Yeazel-Klein, T. R.; Davis, A. G.; Becker, M. L. Thiol-ene-Based 3D Printing of Bioresorbable Fumarate-Based ABA Triblock Copolyester Elastomers. *Adv. Mater. Technol.* **2023**, *8*, No. 2201904.
(17) Wilson, J. A.; Luong, D.; Kleinfehn, A. P.; Sallam, S.; Wesdemiotis, C.; Becker, M. L. Magnesium Catalyzed Polymerization of End Functionalized Poly(propylene maleate) and Poly(propylene fumarate) for 3D Printing of Bioactive Scaffolds. *J. Am. Chem. Soc.* **2018**, *140*, 277−284.
(18) Le Fer, G.; Luo, Y. Y.; Becker, M. L. Poly(propylene fumarate) stars, using architecture to reduce the viscosity of 3D printable resins. *Polym. Chem.* **2019**, *10*, 4655−4664.
(19) Brooks, S.; Merckle, D.; Weems, A. C. 4D Photopolymers Derived From Ring-Opening Copolymerization of Cyclic Anhydrides and Limonene Oxide. *ACS Sustainable Chem. Eng.* **2023**, *11*, 10252−10263.
(20) Abel, B. A.; Lidston, C. A. L.; Coates, G. W. Mechanism-Inspired Design of Bifunctional Catalysts for the Alternating Ring-Opening Copolymerization of Epoxides and Cyclic Anhydrides. *J. Am. Chem. Soc.* **2019**, *141*, 12760−12769.
(21) Xie, R.; Zhang, Y.; Yang, G.; Zhu, X.; Li, B.; Wu, G. Record Productivity and Unprecedented Molecular Weight for Ring-Opening Copolymerization of Epoxides and Cyclic Anhydrides Enabled by Organoboron Catalysts. *Angew. Chem., Int. Ed.* **2021**, *60*, 19253−19261.
(22) Liang, J. X.; Ye, S. X.; Wang, S. Y.; Wang, S. J.; Han, D. M.; Huang, S.; Huang, Z. H.; Liu, W.; Xiao, M.; Sun, L. Y.; Meng, Y. Z. Biodegradable Copolymers from CO2, Epoxides, and Anhydrides Catalyzed by Organoborane/Tertiary Amine Pairs: High Selectivity and Productivity. *Macromolecules* **2022**, *55*, 6120−6130.
(23) Lidston, C. A. L.; Severson, S. M.; Abel, B. A.; Coates, G. W. Multifunctional Catalysts for Ring-Opening Copolymerizations. *ACS Catal.* **2022**, *12*, 11037−11070.
(24) Gregory, G. L.; Williams, C. K. Exploiting Sodium Coordination in Alternating Monomer Sequences to Toughen Degradable Block Polyester Thermoplastic Elastomers. *Macromolecules* **2022**, *55*, 2290−2299.
(25) West, J. K.; Brennan, A. B.; Clark, A. E.; Zamora, M.; Hench, L. L. Cyclic anhydride ring opening reactions: Theory and application. *J. Biomed. Mater. Res.* **1998**, *41*, 8−17.
(26) Robert, C.; de Montigny, F.; Thomas, C. Tandem synthesis of alternating polyesters from renewable resources. *Nat. Commun.* **2011**, *2*, No. 586.
(27) Rostamian, M.; Kalaee, M. R.; Dehkordi, S. R.; Panahi-Sarmad, M.; Tirgar, M.; Goodarzi, V. Design and characterization of poly(glycerol-sebacate)-co-poly (caprolactone) (PGS-co-PCL) and its nanocomposites as novel biomaterials: The promising candidate for soft tissue engineering. *Eur. Polym. J.* **2020**, *138*, No. 109985.
(28) Todea, A.; Deganutti, C.; Spennato, M.; Asaro, F.; Zingone, G.; Milizia, T.; Gardossi, L. Azelaic Acid: ABio-Based Building Block for Biodegradable Polymers. *Polymers* **2021**, *13*, No. 4091.
(29) Hill, J. W.; Carothers, W. H. Studies of polymerization and ring formation. XIV. A linear superpolyanhydride and a cyclic dimeric anhydride from sebacic acid. *J. Am. Chem. Soc.* **1932**, *54*, 1569−1579.
(30) Li, D. S.; Sha, K.; Li, Y. P.; Wang, S. W.; Wang, J. Y. Synthesis and characterization of triblock copolymer by combining enzymatic condensation polymerization and ATRP. *Chin. Sci. Bull.* **2006**, *51*, 1065−1068.
(31) Perin, G. B.; Felisberti, M. I. Enzymatic Synthesis of Poly(glycerol sebacate): Kinetics, Chain Growth, and Branching Behavior. *Macromolecules* **2020**, *53*, 7925−7935.
(32) Li, J.; Stayshich, R. M.; Meyer, T. Y. Exploiting Sequence To Control the Hydrolysis Behavior of Biodegradable PLGA Copolymers. *J. Am. Chem. Soc.* **2011**, *133*, 6910−6913.
(33) Moore, J. S.; Stupp, S. I. Room-Temperature Polyesterification. *Macromolecules* **1990**, *23*, 65−70.
(34) Rickerby, J.; Prabhakar, R.; Patel, A.; Knowles, J.; Brocchini, S. A biomedical library of serinol-derived polyesters. *J. Controlled Release* **2005**, *101*, 21−34. Proceedings of the Eight European Symposium on Controlled Drug Delivery.
(35) Ortiz, C.; Ferreira, M. L.; Barbosa, O.; dos Santos, J. C. S.; Rodrigues, R. C.; Berenguer-Murcia, A.; et al. Novozym 435: the "perfect" lipase immobilized biocatalyst? *Catal. Sci. Technol.* **2019**, *9*, 2380−2420.
(36) Lidston, C. A. L.; Abel, B. A.; Coates, G. W. Bifunctional Catalysis Prevents Inhibition in Reversible-Deactivation Ring-Open-

https://doi.org/10.1021/acsapm.3c02745
ACS Appl. Polym. Mater. XXXX, XXX, XXX−XXX

ing Copolymerizations of Epoxides and Cyclic Anhydrides. *J. Am. Chem. Soc.* **2020**, *142*, 20161−20169.
(37) Wu, Y. L.; D'Amato, A. R.; Yan, A. M.; Wang, R. Q.; Ding, X. C.; Wang, Y. D. Three-Dimensional Printing of Poly(glycerol sebacate) Acrylate Scaffolds via Digital Light Processing. *ACS Appl. Bio Mater.* **2020**, *3*, 7575−7588.
(38) Setter, R.; Schmölzer, S.; Rudolph, N.; Moukhina, E.; Wudy, K. Thermal stability and curing behavior of acrylate photopolymers for additive manufacturing. *Polym. Eng. Sci.* **2023**, *63*, 2180−2192.
(39) Deacy, A. C.; Gregory, G. L.; Sulley, G. S.; Chen, T. T. D.; Williams, C. K. Sequence Control from Mixtures: Switchable Polymerization Catalysis and Future Materials Applications. *J. Am. Chem. Soc.* **2021**, *143*, 10021−10040.
(40) Zhao, Y.; Yu, M.; Zhang, S.; Wu, Z.; Liu, Y.; Peng, C.-H.; Fu, X. A well-defined, versatile photoinitiator (salen)Co−CO2CH3 for visible light-initiated living/controlled radical polymerization. *Chem. Sci.* **2015**, *6*, 2979−2988.
(41) Zhao, Y.; Zhang, S.; Wu, Z.; Liu, X.; Zhao, X.; Peng, C.-H.; Fu, X. Visible-Light-Induced Living Radical Polymerization (LRP) Mediated by (salen)Co(II)/TPO at Ambient Temperature. *Macromolecules* **2015**, *48*, 5132−5139.
(42) Zhu, S.; Zhao, M.; Zhou, H.; Wen, Y.; Wang, Y.; Liao, Y.; Zhou, X.; Xie, X. One-pot synthesis of hyperbranched polymers via visible light regulated switchable catalysis. *Nat. Commun.* **2023**, *14*, No. 1622.
(43) Rabnawaz, M.; Wyman, I.; Auras, R.; Cheng, S. A roadmap towards green packaging: the current status and future outlook for polyesters in the packaging industry. *Green Chem.* **2017**, *19*, 4737−4753.
(44) Wang, L. J.; Wang, F.; Zhou, Q.; Wang, Y. F.; Song, H. X.; Yang, H. Y. Metal-free Lewis pairs catalysed synthesis of fluorescently labelled polyester-based amphiphilic polymers for biological imaging. *Eur. Polym. J.* **2022**, *166*, No. 111033.
(45) Sanford, M. J.; Carrodeguas, L. P.; Van Zee, N. J.; Kleij, A. W.; Coates, G. W. Alternating Copolymerization of Propylene Oxide and Cyclohexene Oxide with Tricyclic Anhydrides: Access to Partially Renewable Aliphatic Polyesters with High Glass Transition Temperatures. *Macromolecules* **2016**, *49*, 6394−6400.
(46) Chidara, V. K.; Gnanou, Y.; Feng, X. S. Using Triethylborane to Manipulate Reactivity Ratios in Epoxide-Anhydride Copolymerization: Application to the Synthesis of Polyethers with Degradable Ester Functions. *Molecules* **2022**, *27*, 466.
(47) Chen, Y.; Shen, J.; Liu, S.; Zhao, J.; Wang, Y.; Zhang, G. High Efficiency Organic Lewis Pair Catalyst for Ring-Opening Polymerization of Epoxides with Chemoselectivity. *Macromolecules* **2018**, *51*, 8286−8297.
(48) Alagi, P.; Gnanou, Y.; Feng, X. Quasilinear polyglycidols by triethyborane-controlled anionic polymerization of unprotected glycidol. *Chem. Commun.* **2023**, *59*, 2958−2961.
(49) Kummari, A.; Pappuru, S.; Chakraborty, D. Fully alternating and regioselective ring-opening copolymerization of phthalic anhydride with epoxides using highly active metal-free Lewis pairs as a catalyst. *Polym. Chem.* **2018**, *9*, 4052−4062.
(50) Hu, L. F.; Zhang, C. J.; Wu, H. L.; Yang, J. L.; Liu, B.; Duan, H. Y.; Zhang, X. H. Highly Active Organic Lewis Pairs for the Copolymerization of Epoxides with Cyclic Anhydrides: Metal-Free Access to Well-Defined Aliphatic Polyesters. *Macromolecules* **2018**, *51*, 3126−3134, DOI: 10.1021/acs.macromol.8b00499.
(51) Ji, H.-Y.; Chen, X.-L.; Wang, B.; Pan, L.; Li, Y.-S. Metal-free, regioselective and stereoregular alternating copolymerization of monosubstituted epoxides and tricyclic anhydrides. *Green Chem.* **2018**, *20*, 3963−3973.
(52) Chen, Y.; Miller, P. G.; Ding, X. C.; Stowell, C. E. T.; Kelly, K. M.; Wang, Y. D. Chelation Crosslinking of Biodegradable Elastomers. *Adv. Mater.* **2020**, *32*, No. 2003761.
(53) Ma, W.; Ding, X. C.; Chen, Y.; Wang, Y. D. Synthesis and Characterization of Alkyne-Functionalized Photo-Cross-Linkable Polyesters. *Acs Omega* **2022**, *7*, 15540−15546.
(54) Yeh, Y. C.; Ouyang, L. L.; Highley, C. B.; Burdick, J. A. Norbornene-modified poly(glycerol sebacate) as a photocurable and biodegradable elastomer. *Polym. Chem.* **2017**, *8*, 5091−5099.
(55) Ding, X.; Wu, Y. L.; Gao, J.; Wells, A.; Lee, K.; Wang, Y. Tyramine functionalization of poly(glycerol sebacate) increases the elasticity of the polymer. *J. Mater. Chem. B* **2017**, *5*, 6097−6109.
(56) Zamboulis, A.; Nakiou, E. A.; Christodoulou, E.; Bikiaris, D. N.; Kontonasaki, E.; Liverani, L.; Boccaccini, A. R. Polyglycerol Hyperbranched Polyesters: Synthesis, Properties and Pharmaceutical and Biomedical Applications. *Int. J. Mol. Sci.* **2019**, *20*, No. 6210.
(57) Ding, X.; Chen, Y.; Chao, C. A.; Wu, Y. L.; Wang, Y. Control the Mechanical Properties and Degradation of Poly(Glycerol Sebacate) by Substitution of the Hydroxyl Groups with Palmitates. *Macromol. Biosci.* **2020**, *20*, No. e2000101.
(58) Zhu, Y. Z.; Shen, J.; Yin, L.; Wei, X. J.; Chen, F.; Zhong, M. Q.; Gu, Z.; Xie, Y.; Jin, W.; Liu, Z. J.; Chitrakar, C.; Chang, L. Q. Directly photopatterning of polycaprolactone-derived photocured resin by UV-initiated thiol-ene "click" reaction: Enhanced mechanical property and excellent biocompatibility. *Chem. Eng. J.* **2019**, *366*, 112−122.
(59) Ligon, S. C.; Liska, R.; Stampfl, J.; Gurr, M.; Mulhaupt, R. Polymers for 3D Printing and Customized Additive Manufacturing. *Chem. Rev.* **2017**, *117*, 10212−10290.
(60) Oesterreicher, A.; Gorsche, C.; Ayalur-Karunakaran, S.; Moser, A.; Edler, M.; Pinter, G.; Schlogl, S.; Liska, R.; Griesser, T. Exploring Network Formation of Tough and Biocompatible Thiol-yne Based Photopolymers. *Macromol. Rapid Commun.* **2016**, *37*, 1701−1706.
(61) Constant, E.; King, O.; Weems, A. C. Bioderived 4D Printable Terpene Photopolymers from Limonene and beta-Myrcene. *Biomacromolecules* **2022**, *23*, 2342−2352.
(62) Fritschen, A.; Bell, A. K.; Konigstein, I.; Stuhn, L.; Stark, R. W.; Blaeser, A. Investigation and comparison of resin materials in transparent DLP-printing for application in cell culture and organs-on-a-chip. *Biomater. Sci.* **2022**, *10*, 1981−1994.
(63) Kinstlinger, I. S.; Saxton, S. H.; Calderon, G. A.; Ruiz, K. V.; Yalacki, D. R.; Deme, P. R.; Rosenkrantz, J. E.; Louis-Rosenberg, J. D.; Johansson, F.; Janson, K. D.; Sazer, D. W.; Panchavati, S. S.; Bissig, K.-D.; Stevens, K. R.; Miller, J. S. Generation of model tissues with dendritic vascular networks via sacrificial laser-sintered carbohydrate templates. *Nat. Biomed. Eng.* **2020**, *4*, 916−932.
(64) Jiao, Y.-P.; Cui, F.-Z. Surface modification of polyester biomaterials for tissue engineering. *Biomed. Mater.* **2007**, *2*, R24.
(65) Luo, H. T.; Zhou, Y. B.; Li, Q. T.; Zhang, B. R.; Cao, X. D.; Zhao, J. P.; Zhang, G. Z. Oxygenated Boron Species Generated In Situ by Protonolysis Enables Precision Synthesis of Alternating Polyesters. *Macromolecules* **2023**, *56*, 1907−1920.

https://doi.org/10.1021/acsapm.3c02745
ACS Appl. Polym. Mater. XXXX, XXX, XXX−XXX